Journal of Materials Chemistry B

ROYAL SOCIETY OF CHEMISTRY

PAPER

View Article Online
View Journal | View Issue

Cite this: J. Mater. Chem. B, 2022, 10, 8058

Highly efficient discrimination of cancer cells based on *in situ*-activated phosphorescence energy transfer for targeted cell imaging†

Yao-Hua Liu[abc] and Yu Liu *[abc]

Received 14th July 2022,
Accepted 2nd September 2022

DOI: 10.1039/d2tb01494g

rsc.li/materials-b

Highly efficient discrimination between cancer cells and normal cells is full of challenges for precise diagnosis. Herein, we report an effective *in situ*-activated phosphorescence energy transfer supramolecular assembly constructed by a bromophenyl pyridine derivative (BPPY), cucurbit[8]uril (CB[8]), and rhodamine B-grafted hyaluronic acid (HAR) through noncovalent interaction. As compared with BPPY, CB[8] encapsulated two BPPY molecules, resulting in a biaxial pseudorotaxane supramolecular assembly showing purely organic room-temperature phosphorescence induced by macrocyclic confinement, which when further co-assembled with HAR, formed a multivalent supramolecular assembly with phosphorescence energy transfer. Benefitting from the targeting of hyaluronic acid and the cyclolactam ring ON–OFF reaction of HAR, such supramolecular assembly with an open ring presents red delayed fluorescence through phosphorescence energy transfer in cancer cells, while the assembly showed only green phosphorescence in normal cells, realizing highly efficient discrimination between cancer and normal cells. This supramolecular assembly is responsive to the physiological environment and provides a supramolecular platform for precise diagnosis.

Introduction

Supramolecular multistep assemblies widely exist in nature, with stable and ordered structures that give rise to attractive physical and chemical properties.[1–4] Many researchers use various weak interactions to construct artificial supramolecular multistep assemblies to simulate natural systems for biosensing and imaging,[5,6] drug delivery,[7–9] smart biomaterials,[10,11] and biomimetics systems.[12] In particular, bioimaging, as an important method to understand the structure and physiological activities of biological tissues, has played an indispensable role in scientific research and clinical diagnosis.[13,14] Taking into account phosphorescence, characterized by the involvement of triplet states, long emission lifetime and large Stokes shift, water-soluble phosphorescent or time-lapse fluorescent materials can have a high signal-to-noise ratio, achieving accurate bioimaging.[15–18] As a consequence, room-temperature phosphorescence (RTP) in aqueous solution, emitted by purely organic molecules, has attracted great interest from chemical and biological researchers.[19] However, most RTP materials are solid-state and water-insoluble, while the amorphous RTP systems in aqueous solution are seriously affected by quenching from oxygen and water.[20] Despite these difficulties, researchers persisted in their efforts and have successfully developed a variety of RTP systems in aqueous solution.[19,21,22] For example, we have constructed a purely organic supramolecular pseudorotaxane polymer with ultra-long RTP lifetime for use in cancer cell targeted imaging.[23]

On the other hand, stimuli-responsive smart materials have attracted special attention from researchers.[24,25] These systems can respond to endogenous or exogenous stimuli and produce dynamic responses, changing their structure or assembly behaviour, thereby achieving functional changes.[26] Well-designed responsive supramolecular assemblies can ultimately be used in a wide range of biomedical applications.[24,27,28] For example, our group reported a photooxidation-driven anthracene bromophenyl pyridine for the targeted imaging of dual organelles in living cells[29] and a photosensitive self-cleaving supramolecular assembly for photodynamic therapy.[30] However, the design and construction of supramolecular optical probes for high-sensitivity discrimination of cancer cells and normal cells remain a great challenge. Especially, purely organic RTP and delayed-fluorescence supramolecular optical probe systems that respond to the physiological environment and achieve efficient discrimination between cancer cells and normal cells have rarely been reported.

Herein, we report a phosphorescent/delayed-fluorescence supramolecular secondary assembly responsive to the physiological

[a] College of Chemistry, State Key Laboratory of Elemento-Organic Chemistry, Nankai University, Tianjin 300071, China. E-mail: yuliu@nankai.edu.cn
[b] Haihe Laboratory of Sustainable Chemical Transformations, Tianjin 300192, China
[c] Collaborative Innovation Center of Chemical Science and Engineering (Tianjin), Tianjin 300072, China

† Electronic supplementary information (ESI) available. See DOI: https://doi.org/10.1039/d2tb01494g

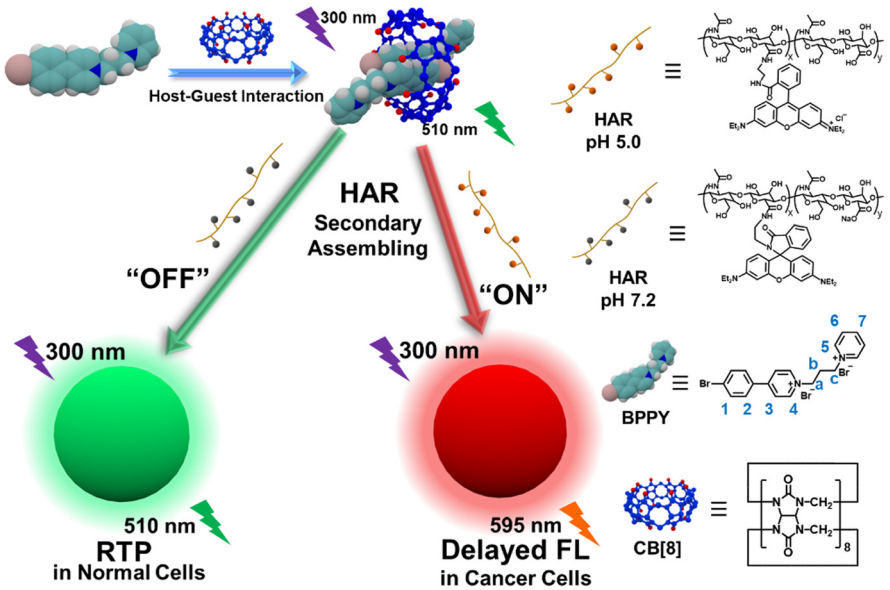

Scheme 1 Schematic illustration of the supramolecular nanoparticle response to the physiological environment, with green phosphorescence in normal cells and red delayed fluorescence in cancer cells.

environment, constructed by a dicationic bromophenyl pyridinium derivative (BPPY), cucurbit[8]uril (CB[8]), and rhodamine B-grafted hyaluronic acid (HAR) (Scheme 1). The bromophenyl pyridinium derivative BPPY interacted with CB[8] by host–guest interaction to form a complex. Benefitting from the strong affinity and macrocyclic confinement effect of CB[8], the dicationic guest BPPY (without phosphorescence) formed a complex with CB[8], which exhibited good water solubility and efficient RTP in aqueous solution. The complex further assembled with HAR by electrostatic action to form supramolecular nanoparticles. Notably, this supramolecular secondary assembly emitted orange-red delayed fluorescence through phosphorescence energy transfer at pH 5.0, but only green phosphorescence at pH 7.2. Benefitting from the targeting properties of hyaluronic acid, the supramolecular ternary assemblies can efficiently enter cancer cells, but not normal cells, and activate phosphorescence energy transfer in lysosomes, achieving delayed fluorescence for accurate cancer cell imaging. While the supramolecular complex of BPPY⊂CB[8] lacks the targeting ability of cancer cells, the complex can enter normal cells and exhibit green phosphorescence, achieving highly efficient discrimination of cancer and normal cells. Such supramolecular assembly responsive to the physiological environment provides a supramolecular platform for precise diagnosis.

Results and discussion

We synthesized a bromophenyl pyridinium derivative (BPPY) as guest molecule and rhodamine B-grafted hyaluronic acid (Fig. S1–S5, ESI†). Firstly, the binding behaviors of BPPY and two kinds of CBs (CB[7] and CB[8]) were studied. The nuclear magnetic resonance (NMR) spectra of BPPY changed significantly with the addition of CBs, indicating that there was strong host–guest interaction between BPPY and the CBs (Fig. 1a and b). Then, ^{1}H–^{1}H COSY spectra were carried out to determine the attribution of proton signals (Fig. S6 and S7, ESI†). Specifically, protons located on bromophenyl pyridinium were shifted upfield with the addition of CB[7]. The chemical shift of the proton located on pyridinium at the other end was almost unchanged, indicating that it was outside the cavity of CB[7]. Unlike the case of CB[7], the ^{1}H NMR spectra of BPPY showed a typical phenomenon of slow exchange with the addition of CB[8]. Compared with free BPPY, H_1, H_2, H_3 and H_4 located on the bromophenyl pyridinium of BPPY⊂CB[8] were upshifted 1.21, 0.93, 0.91 and 0.07 ppm, while H_5 located on the pyridine unit and H_b located on the alkyl chain were downshifted 0.12 and 0.14 ppm, respectively.

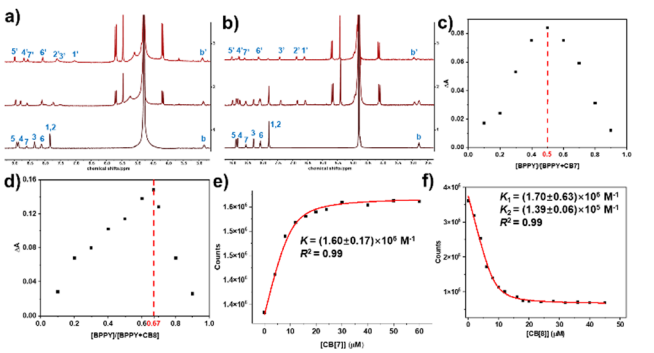

Fig. 1 (a) ^{1}H NMR spectroscopy of BPPY with (i) 0, (ii) 0.5 and (iii) 1 eq. CB[7] in D_2O at 298 K; (b) ^{1}H NMR spectroscopy of BPPY with (i) 0, (ii) 0.25 and (iii) 0.5 eq. CB[8] in D_2O at 298 K; (c) Job's plot of BPPY and CB[7] in PBS solution ([BPPY] + [CB[7]] = 50 μM) at 298 K; (d) Job's plot of BPPY and CB[8] in PBS solution ([BPPY] + [CB[8]] = 50 μM) at 298 K; (e) nonlinear least-squares fit of the change in absorption of BPPY as a function of CB[7] concentration in PBS solution at 298 K; (f) nonlinear least-squares fit of the change in absorption of the BPPY as a function of CB[8] concentration in PBS solution at 298 K.

These experimental results proved that CB[7] and CB[8] were both encapsulated with the bromophenyl pyridine group. In addition, the binding ratio of BPPY to CB[8] can be preliminarily confirmed by ^{1}H NMR spectrum as 2 : 1, because of the slow exchange phenomenon (Fig. S8, ESI†). Next, we studied the binding ratio and binding constants of BPPY with CB[7] or CB[8].

The Job plot experiments carried out using the UV-vis absorption spectra showed that BPPY can form a complex with CB[7] at the ratio of 1 : 1 (Fig. 1c), while it forms a complex with CB[8] at the ratio of 2 : 1 (Fig. 1d). Accompanied by the addition of CB[7] or CB[8], the band at 310 nm in the UV-vis spectrum of BPPY gradually decreased and exhibited a slight red shift (Fig. S9, ESI†).

The binding constant K_s value for the inclusion complex of BPPY⊂CB[7] was determined to be $(1.60 \pm 0.17) \times 10^7$ M^{-1} according to the titration curve, which was well fitted with the equation for 1 : 1 host–guest complex (Fig. 1e). The binding constant K_1 and K_2 values of BPPY⊂CB[8] were calculated to be $(1.70 \pm 0.63) \times 10^6$ and $(1.39 \pm 0.06) \times 10^5$ M^{-1}, respectively, using a nonlinear least-squires method (Fig. 1f).

Subsequently, we studied the optical properties of BPPY⊂CB[7] and BPPY⊂CB[8]. To be specific, there was an emission peak only at about 380 nm for BPPY alone. With the addition of CB[7], the emission peak at 380 nm was slightly enhanced (Fig. S10, ESI†). The fluorescence and time-delayed photoluminescent spectra of BPPY⊂CB[7] were then tested, which showed that the emission peak at 380 nm was fluorescent emission, and BPPY⊂CB[7] had no phosphorescent emission (Fig. S11, ESI†). As for CB[8], the emission peak at 380 nm was greatly reduced, and a new emission peak appeared at about 510 nm (Fig. 2a). The emission peak at 380 nm should be attributed to fluorescence emission according to the fluorescence spectrum of BPPY⊂CB[8] (Fig. 2b). Excitingly, time-lapse photoluminescence spectra preliminarily confirm that BPPY⊂CB[8] had room-temperature phosphorescent emission at 510 nm (Fig. 2c). To further confirm phosphorescence of BPPY⊂CB[8] and rule out the possibility of thermally activated delayed fluorescence, we tested the photoluminescence spectra of BPPY⊂CB[8] under argon and low temperature (Fig. S12, ESI†). Moreover, the phosphorescence lifetime and quantum yield were measured to be 377.15 μs and 2.80% (Fig. 2d and Fig. S13, ESI†). The experimental results verified that BPPY⊂CB[8] had room-temperature phosphorescent emission in aqueous solution under atmospheric conditions.

This green room-temperature phosphorescent emission may be suitable for energy transfer from the complex to the rhodamine B derivative. Therefore, we synthesized two kinds of 2-(2-aminoethyl) rhodamine B amides and grafted them onto hyaluronic acids with different degrees of modification and molecular weight (HAR and HAR2, Fig. S4 and S5, ESI†), which can form supramolecular ternary assemblies with BPPY⊂CB[8] through electrostatic action. Firstly, dynamic light scattering (DLS), zeta potential and transmission electron microscope (TEM) experiments were carried out to study the co-assembly behaviour of BPPY⊂CB[8] and HAR. The complex of BPPY⊂CB[8] gave a positive surface potential value at first, then the addition of HAR caused the supramolecular ternary assembly to exhibit a negative potential value, indicating that anionic HAR was distributed on the surface of BPPY⊂CB[8] (Fig. 3a and b). TEM images showed that the supramolecular ternary assembly presented spherical nanoparticles in the size of hundreds of nanometres (Fig. 3c). DLS experiments showed that the assembly had a hydrodynamic diameter range of 350–650 nm (Fig. 3d). Besides this, TEM and DLS experiments showed that BPPY⊂CB[8] and HAR2 formed smaller supramolecular nanoparticles with the diameter of about

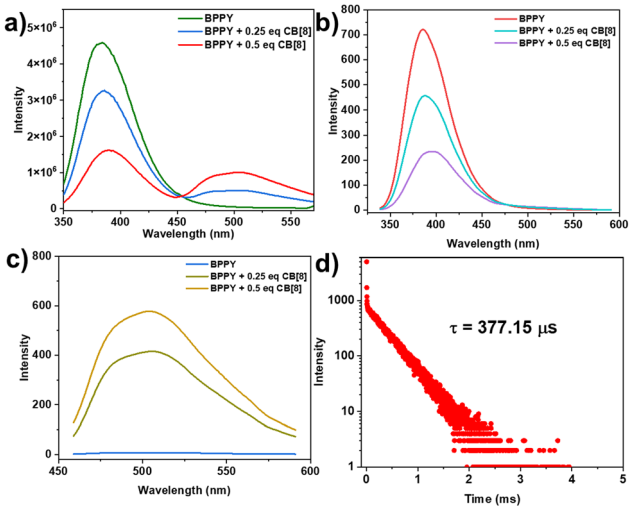

Fig. 2 (a) Photoluminescence spectra of BPPY (10 μM) and CB[8] at the concentrations of 0, 2.5 and 5 μM (excitation = 320 nm); (b) fluorescence spectra of BPPY (10 μM) and CB[8] at concentrations of 0, 2.5 and 5 μM (excitation = 320 nm); (c) time-lapse photoluminescence spectra (delayed by 0.2 ms) of BPPY (10 μM) and CB[8] at concentrations of 0, 2.5 and 5 μM (excitation = 320 nm); (d) time-resolved photoluminescence decay curves of BPPY⊂CB[8] at 505 nm ([BPPY] = 2[CB[8]] = 10 μM, excitation = 320 nm).

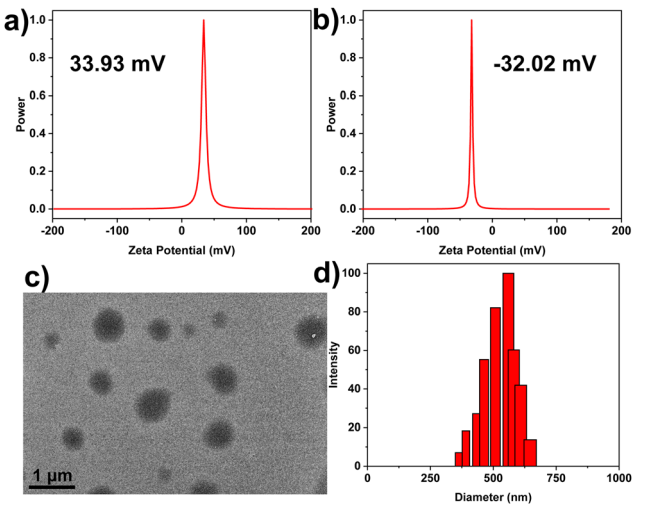

Fig. 3 (a) Zeta potential of BPPY⊂CB[8] in PBS solution; (b) Zeta potential of BPPY⊂CB[8]@HAR in PBS solution; (c) TEM image of BPPY⊂CB[8]@HAR; (d) DLS data of BPPY⊂CB[8]@HAR in PBS solution.

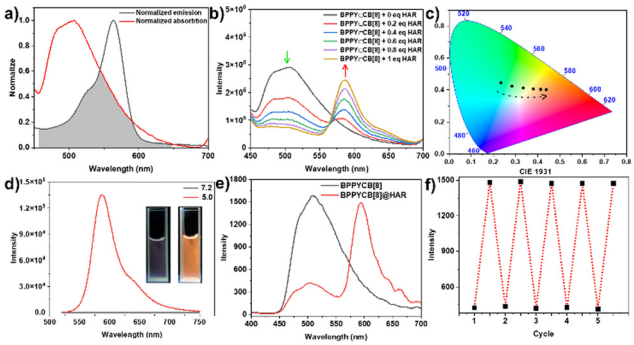

Fig. 4 (a) Normalized absorption spectrum of HAR and emission spectrum of BPPY⊂CB[8]; (b) photoluminescent spectra of BPPY⊂CB[8] in the presence of different ratios of HAR ([BPPY] = 2CB[8] = 10 μM, excitation = 320 nm); (c) CIE chromaticity diagram showing the photoluminescence color changes of BPPY⊂CB[8] with the addition of HAR; (d) fluorescent emission spectra of HAR at pH 5.0 and 7.2 (excitation = 500 nm); (e) time-lapse photoluminescence spectra (delayed 0.2 ms) of BPPY⊂CB[8]@HAR at pH 5.0 and 7.2 (excitation = 320 nm); (f) variation of the emission of BPPY⊂CB[8]@HAR at 595 nm at alternative pH 5.0 and 7.2.

120 nm (Fig. S14, ESI†). Therefore, a supramolecular nanoparticle was successfully constructed by the secondary assembly method.

Next, we studied the optical properties of the supramolecular ternary assembly BPPY⊂CB[8]@HAR at pH 5.0. The emission spectrum of BPPY⊂CB[8] overlapped well with the absorption spectrum of HAR, indicating that it had the prerequisite for energy transfer (Fig. 4a). Subsequently, the energy transfer process between BPPY⊂CB[8] and HAR was detected by fluorescence titration experiment (Fig. 4b and c). With the addition of HAR, the phosphorescence of BPPY⊂CB[8] gradually decreased. At the same time, fluorescence around 595 nm from HAR was present and gradually increased. In the supramolecular ternary assemblies, the energy transfer efficiency from BPPY⊂CB[8] to HAR reached 75%. Compared to HAR, the energy transfer efficiency of smaller supramolecular nanoparticles constructed by BPPY⊂CB[8] and HAR2 was slightly improved to 78% (Fig. S15, ESI†). In addition, time-resolved photoluminescence spectra (delay 0.2 ms) of the BPPY⊂CB[8] with and without the addition of HAR also confirmed the process of phosphorescence energy transfer (Fig. 4d). On the other hand, the lifetime of the reference assembly constructed by BPPY⊂CB[8] and HA at 510 nm was 1017 μs according to the time-resolved photoluminescence decay curves (Fig. S16, ESI†), while the lifetime of BPPY⊂CB[8]@HAR was 397 μs at 510 nm and 135 μs at 595 nm (Fig. S17, ESI†). Such decrease of lifetime at 510 nm indicated that BPPY⊂CB[8], with phosphorescence, endows the HAR with a longer lifetime *via* an efficient triplet-to-singlet Förster resonance energy transfer (TS-FRET).

As we know, under acidic pH conditions, rhodamine gives strong fluorescence when the cyclolactam ring opens, but the emission is dramatically reduced at basic or neutral pH, triggered by ring closure.[31] Thus, we speculated that the supramolecular ternary assembly can also respond to pH. The UV-vis absorption and fluorescence spectra of HAR at weak acid and neutral pH were first investigated. In the case of pH 5.0, HAR had an absorption peak at about 563 nm, while this absorption peak decreased and almost completely disappeared at pH 7.2 (Fig. S18, ESI†). Correspondingly, the solution of HAR changed from pink to colourless. Fluorescence spectra showed RhB derivatives have no fluorescence at pH 7.2, while the cyclolactam ring of the rhodamine unit in HAR opened under weak acid condition (pH 5.0), showing fluorescence (Fig. 4e); meanwhile the fluorescence intensity increased as pH value decreased to give the pK_a value of 5.1 (Fig. S19, ESI†).[31] Therefore, HAR can act as an acceptor for phosphorescence energy transfer. Based on the above experimental results, we speculate that the supramolecular ternary assembly could achieve phosphorescence or time-delayed fluorescence emission by adjusting pH. The ability of HAR to respond to pH with fluorescence was tested by alternately adding hydrochloric acid and sodium hydroxide (Fig. 4f). Within five cycles, the fluorescence of HAR was not significantly attenuated, indicating it had good stability and repeatability. As expected, the supramolecular ternary assembly had green phosphorescence at pH 7.2 and orange-red delayed fluorescence at pH 5.0.

Usually, organelles of cells have different pH values; for example, lysosomes are slightly acidic, while mitochondria and the cytosol both are slightly basic. Considering the supramolecular assembly's excellent ability to respond to pH, we investigated its potential application to targeted cell imaging. As a cell imaging agent, low toxicity and good biocompatibility are essential. Thus, the cytotoxicity of the supramolecular ternary assembly of BPPY⊂CB[8]@HAR was examined using human non-small-cell lung cancer (A549) cells and human kidney (293T) cells using a standard cell counting kit-8 (CCK-8) analysis. The experimental results showed that the supramolecular ternary assembly had good safety thanks to the excellent biocompatibility of HA, and the cell survival rate was still greater than 90% even when the concentration was as high as 50 μM (Fig. S20, ESI†). Subsequently, we examined the ability of this assembly for cell imaging by confocal laser scanning microscopy (CLSM). For A549 cells incubated with BPPY⊂CB[8] and HAR successively, weak green phosphorescence and bright-orange-red time-lapse fluorescence was observed (Fig. 5a). Furthermore, subcellular distribution of such supramolecular assembly was investigated by co-staining with a commercial Lyso-Tracker blue. Remarkably, the orange-red emission signal assigned to BPPY⊂CB[8]@HAR displayed good overlap with the blue region of Lyso-Tracker blue, indicating that such supramolecular ternary assembly was specifically distributed in lysosomes (Fig. S21, ESI†). As a control, for A549 cells incubated with BPPY⊂CB[8], only effective green phosphorescence was observed (Fig. 5b). In addition, a microplate reader was also used to quantitatively analyse the time-resolved luminescence signal. Results showed two endpoints assigned to 510 nm and 595 nm; both presented the corresponding emission with a delay of 50 μs after incubation with cells for 24 h (Fig. S22, ESI†). Compared with A549 cells, the normal cells (293T cells) incubated with BPPY⊂CB[8] and HAR successively showed green luminescence emission because of the targeting properties of hyaluronic acid (Fig. 5c). Moreover, confocal images and flow cytometry of living A549 cells and 293T cells in a same cell culture dish further confirmed the ability of the supramolecular assembly

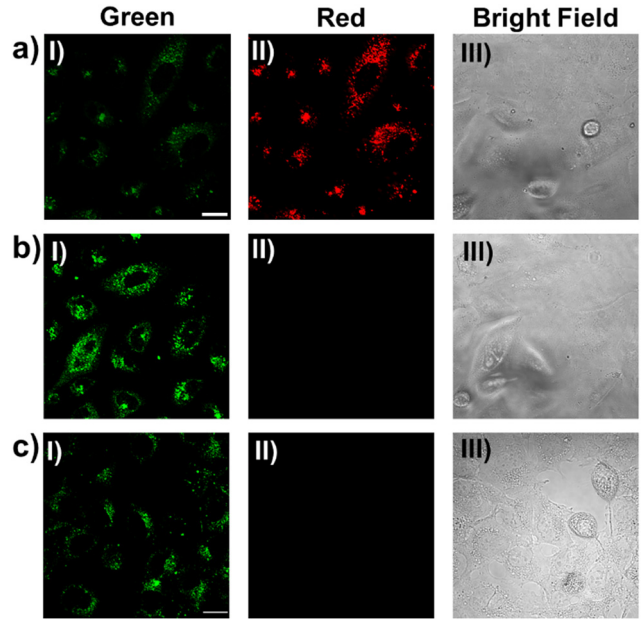

Fig. 5 (a) Confocal images of living A549 cells incubated with BPPY⊂CB[8] and HAR successively; (b) confocal images of living A549 cells incubated with only BPPY⊂CB[8]; (c) confocal images of living 293T cells incubated with BPPY⊂CB[8] and HAR successively (scale bar = 20 μm). Figures labelled (I), green channel corresponding to the phosphorescent emission; (II), red channel corresponding to the delayed fluorescent emission; (III) images of cells in bright field. The excitation wavelength for the green and red channels was 405 nm, and the emission wavelength ranges for the green and red channels were 450–550 and 570–670 nm, respectively.

to discriminate cancer cells from normal cells (Fig. S23 and S24, ESI†). As a control, 293T cells incubated with BPPY⊂CB[8] also showed green luminescence emission (Fig. S25, ESI†). Therefore, this supramolecular ternary assembly of BPPY⊂CB[8]@HAR had the ability to target lysosomes in cancer cells and activate phosphorescence energy transfer *in situ*, achieving time-lapse fluorescence for accurate cancer cell imaging.

Conclusion

In conclusion, we have constructed a phosphorescence/delayed-fluorescence supramolecular ternary assembly by the strategy of secondary assembly. The guest molecule BPPY and host molecule CB[8] interacted to form a complex with effective room-temperature phosphorescent emission through the host–guest interaction. Such complex was further assembled with HAR to form supramolecular nanoparticles by electrostatic action. Benefitting from the targeting of hyaluronic acid and the cyclolactam ring of HAR activated in cancer cells, such supramolecular assembly presents delayed red fluorescence through phosphorescence energy transfer in the lysosome, while the complex BPPY⊂CB[8] showed only green phosphorescence in normal cells, realizing highly efficient discrimination between cancer and normal cells. We believe that this work provides a simple and effective new way to construct smart phosphorescent materials for precise bioimaging and diagnosis.

Experiment

Synthesis of BPPY

4-(4-Bromophenyl)-1-(3-bromopropyl)pyridinium[32] (100 mg, 1 mmol) was dissolved in dry DMF (30 mL), and pyridine (1 mL) was added dropwise to the reaction solution. Then, the solution was stirred at 375 K overnight. The resulting suspension was filtered, and the precipitate was washed with CH_3CN and ethyl ether. Then, the precipitate dried in vacuum yielding the BPPY as white solid (70 mg, 63%).

^{1}H NMR: (400 MHz, D_2O) δ = 8.88 (d, J = 6.8 Hz, 2H), 8.83 (d, J = 6.8 Hz, 2H), 8.55 (t, J = 8.0 Hz, 1H), 8.29 (d, J = 6.8 Hz, 2H), 8.07 (t, J = 7.6 Hz, 2H), 7.76–7.81 (m, 4H), 4.73–4.77 (m, 4H), 2.75–2.83 (m, 2H) ppm. ^{13}C NMR (101 MHz, DMSO-d_6) δ = 154.20, 146.31, 145.62, 145.48, 133.16, 130.66, 128.68, 126.80, 125.03, 57.93, 57.14, 32.21 ppm. HRMS (m/z): (ESI, H_2O) calculated for $[M\text{-}2Br^-]^{2+}$: 177.0361, found 177.0362.

Synthesis of HAR

Hyaluronic acid (0.5 g, 1.32 mmol) was dissolved in 50 mL DMSO at 60 °C. After the polymer was completely dissolved, the solution was cooled to room temperature. Then, triethylamine (0.92 mL, 6.6 mmol) was added, and the reaction solution was stirred for a further 10 min. At this moment, PyBop (2.6 g, 5.0 mmol) was added, and the mixture was kept stirring at room temperature for 1 h. Rhodamine B ethylenediamine[33] (320 mg, 0.66 mmol) was added, and the reaction mixture was allowed to stir at room temperature for 24 h. Afterwards, the solution was diluted with 50 mL water and then dialyzed against deionized water for under acidic conditions for 7 days (M_w cutoff = 8–14 kDa). After dialysis, the sample was freeze-dried as pink powder.

Author contributions

Y. H. L. synthesized the compounds, performed experiments, collected data, summarized, and wrote the work. The project was edited and supervised by Y. L.

Conflicts of interest

The authors declare no competing interests.

Acknowledgements

This work was financially supported by the National Natural Science Foundation of China (grants 22131008), the Fundamental Research Funds for the Central Universities and the Haihe Laboratory of Sustainable Chemical Transformations.

Notes and references

1 G. M. Whitesides and B. Grzybowski, *Science*, 2002, **295**, 2418–2421.
2 P. Frederix, I. Patmanidis and S. J. Marrink, *Chem. Soc. Rev.*, 2018, **47**, 3470–3489.

3 D. Pochan and O. Scherman, *Chem. Rev.*, 2021, **121**, 13699–13700.
4 Z. Liu, X. Dai, Y. Sun and Y. Liu, *Aggregate*, 2020, **1**, 31–44.
5 J. Li, J. Wang, H. Li, N. Song, D. Wang and B. Z. Tang, *Chem. Soc. Rev.*, 2020, **49**, 1144–1172.
6 T. D. Ashton, K. A. Jolliffe and F. M. Pfeffer, *Chem. Soc. Rev.*, 2015, **44**, 4547–4595.
7 M. Tang, Y.-H. Liu, X.-M. Xu, Y.-M. Zhang and Y. Liu, *Bioorg. Med. Chem.*, 2022, **57**, 116649.
8 M. J. Webber and R. Langer, *Chem. Soc. Rev.*, 2017, **46**, 6600–6620.
9 P. Xing and Y. Zhao, *Small Methods*, 2018, **2**, 1700364.
10 Y.-H. Liu and Y. Liu, *J. Mater. Chem. B*, 2022, **10**, 958–965.
11 P. Xing and Y. Zhao, *Adv. Mater.*, 2016, **28**, 7304–7339.
12 Y.-H. Liu, Y.-M. Zhang, H.-J. Yu and Y. Liu, *Angew. Chem., Int. Ed.*, 2021, **60**, 3870–3880.
13 J. Qian and B. Z. Tang, *Chem*, 2017, **3**, 56–91.
14 K. Heinzmann, L. M. Carter, J. S. Lewis and E. O. Aboagye, *Nat. Biomed. Eng.*, 2017, **1**, 697–713.
15 X. Zhen, Y. Tao, Z. An, P. Chen, C. Xu, R. Chen, W. Huang and K. Pu, *Adv. Mater.*, 2017, **29**, 1606665.
16 J. Wang, Z. Huang, X. Ma and H. Tian, *Angew. Chem., Int. Ed.*, 2020, **59**, 9928–9933.
17 X.-F. Wang, H. Xiao, P.-Z. Chen, Q.-Z. Yang, B. Chen, C.-H. Tung, Y.-Z. Chen and L.-Z. Wu, *J. Am. Chem. Soc.*, 2019, **141**, 5045–5050.
18 Y. Wang, H. Gao, J. Yang, M. Fang, D. Ding, B.-Z. Tang and Z. Li, *Adv. Mater.*, 2021, **33**, e2007811.
19 X.-K. Ma and Y. Liu, *Acc. Chem. Res.*, 2021, **54**, 3403–3414.
20 X. Yan, H. Peng, Y. Xiang, J. Wang, L. Yu, Y. Tao, H. Li, W. Huang and R. Chen, *Small*, 2022, **18**, e2104073.
21 H. Nie, Z. Wei, X.-L. Ni and Y. Liu, *Chem. Rev.*, 2022, **122**, 9032–9077.
22 Y.-H. Liu, M. Tang, X. Zhou and Y. Liu, *Mater. Adv.*, 2022, **3**, 4693–4698.
23 W.-L. Zhou, Y. Chen, Q. Yu, H. Zhang, Z.-X. Liu, X.-Y. Dai, J.-J. Li and Y. Liu, *Nat. Commun.*, 2020, **11**, 4655.
24 Y.-M. Zhang, Y.-H. Liu and Y. Liu, *Adv. Mater.*, 2020, **32**, e1806158.
25 T. Kakuta, T. A. Yamagishi and T. Ogoshi, *Acc. Chem. Res.*, 2018, **51**, 1656–1666.
26 E. Moulin, L. Faour, C. C. Carmona-Vargas and N. Giuseppone, *Adv. Mater.*, 2020, **32**, e1906036.
27 S. Mura, J. Nicolas and P. Couvreur, *Nat. Mater.*, 2013, **12**, 991–1003.
28 P. Li, Y. Chen and Y. Liu, *Chin. Chem. Lett.*, 2019, **30**, 1190–1197.
29 H.-J. Yu, Q. Zhou, X. Dai, F.-F. Shen, Y.-M. Zhang, X. Xu and Y. Liu, *J. Am. Chem. Soc.*, 2021, **143**, 13887–13894.
30 M. Tang, Y. Song, Y. L. Lu, Y. M. Zhang, Z. Yu, X. Xu and Y. Liu, *J. Med. Chem.*, 2022, **65**, 6764–6774.
31 M. H. Lee, J.-H. Han, J. H. Lee, N. Park, R. Kumar, C. Kang and J. S. Kim, *Angew. Chem., Int. Ed.*, 2013, **52**, 6206–6209.
32 X. K. Ma, W. Zhang, Z. Liu, H. Zhang, B. Zhang and Y. Liu, *Adv. Mater.*, 2021, **33**, e2007476.
33 S. Sun, B. Qiao, N. Jiang, J. Wang, S. Zhang and X. Peng, *Org. Lett.*, 2014, **16**, 1132–1135.